7 Nanotube- or graphene-based nanoarmors

Nicola M. Pugno[1], **Vitor R. Coluci**[2] **and Douglas S. Galvão**[2]
[1]Department of Structural Engineering, Politecnico di Torino, 10129, Torino
Italy; [2]Instituto de Física "Gleb Wataghin", Universidade Estadual de Campinas
C.P. 6165, 13083-970 Campinas, São Paulo, Brazil

Abstract

In this paper, nanoimpacts on hexagonal or crossbar nanotube networks as well as on graphene sheets are investigated by elasticity and finite kinematics or impact molecular dynamic simulations. A transition from bending to stretching by increasing the impact kinetic energy of the nanoprojectile is clearly observed. The analysis suggests that the investigated nanotextures are ideal for designing futuristic nanoarmors.

Correspondence/Reprint request: Dr. Nicola M. Pugno, Department of Structural Engineering, Politecnico di Torino, 10129, Torino, Italy. E-mail: nicola.pugno@polito.it

1. Introduction

Providing massive armor is a relatively simple task, admirably achieved in the past by using steel panels. Nowadays lightweight structures are needed, requiring the use of more sophisticated and composite materials, e.g. for protection against both bullet and knife attacks. For a knife, attachment of an additional hard coating layer, to a backing one of ballistic fabric, is required to blunt the weapon and to stop the reinforcement fibers being cut, producing an "integral" armor [1]. The penetration into a bulk material of indenters of different size, shape, mass and velocity could be investigate thanks to a recent and quite general theory [2]. Multi-hit capability and flexibility introduce other design complications, which requires the use of multiple small tiles to simultaneously reduce damage extension and bending stiffness (e.g. as in a dragon skin©). Moreover, "liquid" armors, impregnated with colloidal suspensions, display the liquid-like ability to stiffen rapidly under a shear stress and thus we see smart strength and stiffness enhancements during impact loading [3,4]. And porous materials could be made even stiffer than their non-porous counterparts [5].

Carbon nanotubes, possessing extremely high dynamic strength and stiffness [4], are thus ideal candidates as nanofiber-reinforcements. Many attempts have been made in order to develop procedures to controllably assemble a large number of single walled carbon nanotubes (SWCNTs) in terms of position and orientation [6-9]. The achievement of such procedures would allow the fabrication of ordered SWCNT networks representing a breakthrough in the "bottom-up" manufacturing approach. The ultimate arrangement involving SWCNTs would be the one where isolated SWCNTs are covalently connected by using X-, Y-, or T-like junctions, forming an highly-ordered network. The controlled fabrication of such nanotextures can allow their use in applications such as sensors, filters, flexible electronic devices, composites, electromechanical actuators and, as we are going to investigate, nanoarmors.

2. Finite kinematics of the elastic impact

Consider a projectile having kinetic energy K impacting at the middle of a cable of length $2l$, cross section area A and elastic modulus E. The transversal displacement at the impact point is $\Delta z = l \tan \vartheta$, where ϑ are the base angles of the triangle shaped cable deformation. The elastic energy stored in the cable is $W = k(\Delta l)^2$, where $k = EA/l$ is the stiffness of half cable and $\Delta l = l(1/\cos \vartheta - 1)$ is its finite stretching. When the projectile is stopped its kinetic energy is fully converted into elastic energy, namely $K = W$. Thus, we find the following nonlinear law between impact kinetic energy and the elastic displacement required to stop the projectile:

$$K = EAl\left(\sqrt{1+\frac{\Delta z^2}{l^2}}-1\right)^2 \approx \frac{EAl}{4}\frac{\Delta z^4}{l^4}$$

(1)

where the last approximation, usually satisfied, is valid for not too large $\Delta z /l$. Thus during stretching, as a first approximation, $K \propto \Delta z^4$.

On the other hand, the classical dependence $K \propto \Delta z^2$ is expected if the cable is substituted by a doubly clamped beam under pure bending. Making the trivial (even if hyperstatic) calculations we find $W = 1/2k\Delta z^2$, where $k = 24EI/l^3$ is the beam bending stiffness and I is its moment of inertia. Accordingly, under bending:

$$K = \frac{12EI}{l}\frac{\Delta z^2}{l^2}$$

(2)

The transition between the two deformation mechanisms takes place around a relative displacement $\Delta z^*/l$ that can be found by equating the two previous expressions; accordingly we derive:

$$\frac{\Delta z^*}{l} = \frac{\sqrt{48}}{\lambda}$$

(3a)

where $\lambda = l/\rho$ defines the structural slenderness and $\rho = \sqrt{I/A}$ is the radius of inertia. The kinetic energy corresponding to the transition can be calculated introducing eq. (3a) into eq. (1) or (2):

$$K^* = 576\frac{EAl}{\lambda^4}$$

(3b)

Thus, the model predicts that for $K < K^*$, or $\Delta z < \Delta z^*$, bending prevails and $K \propto \Delta z^2$, whereas for $K > K^*$, or $\Delta z > \Delta z^*$, stretching prevails and $K \propto \Delta z^4$. Note that the transition is mainly dictated by the fiber slenderness.

The maximum kinetic energy corresponding to the stretching failure, arising when the maximum admissible strain ε_{max} (or stress $\sigma_{max} = E\varepsilon_{max}$) is reached, is predicted to be:

$$K_{max} = EAl\varepsilon_{max}^2$$

(4)

whereas for bending we find:

$$K_{max} = \frac{4}{3}\frac{EIl}{h^2}\varepsilon_{max}^2$$

(5)

in which h denotes the height of the beam. Note that their ratio is $3h^2/(4\rho^2)$.

Finally, denoting by n the number of fibers activated during the impact, depending on the geometry of the texture and on the projectile size, the total

kinetic energy would become $K(n) = nK(1)$. For example, for a projectile having cross-section area q and impacting on a texture composed by orthogonal fibers with spacing p, $n \approx 2\left(\sqrt{q}/p+1\right)$.

3. Impact molecular dynamic simulations

The mechanical properties of ordered SWCNT networks have been investigated using impact molecular dynamics simulations [10]. These atomistic simulations were carried out to study the dynamical responses of the network to external colliding objects. The adaptive intermolecular reactive empirical bond-order (AIREBO) potential developed by Stuart *et al*. [11] was used to model carbon-carbon interactions. AIREBO is similar to the reactive potential developed by Brenner [12] but it incorporates by suitable modifications the non-bonded interactions through an adaptative treatment of the intermolecular interactions. This kind of reactive potentials have been proved to be accurate to describe carbon nanotube deformations under mechanical strain [13].

In additional to a classical graphene sheet, two types of SWCNT networks were considered: crossbar and hexagonal configurations. The networks are constructed using one single type of carbon nanotube connected by junctions being labelled as Cb@(*n,m*) and Hex@(*n,m*), for crossbar and hexagonal networks formed by (*n,m*) SWCNTs, respectively. In this work the nanotubes were connected using junctions constructed using 5- and 7- [14] and 5- and 8- [15] membered rings for (6,0) and (8,0) SWCNTs, respectively. Besides the nanotube type, the networks are characterized by the length a and b of the characteristic unit cell, and by the angle γ, with $\gamma=90^{o}$ and $\gamma=60^{o}$ for crossbar and hexagonal networks, respectively [10].

The networks used in the impact studies have a circular target shape with radius R=19nm, with the atoms at the outmost (width ~0.5nm) kept fixed during the simulations. The remaining regions are maintained at the temperature of 300K by using the rescaling velocity method. We have used Hex@(6,0) (a=b=4.75nm, 25376 atoms, Figure 1a and Cb@(6,0) (a=2.91nm and b=2.99nm, 39259 atoms, Figure 1b; or a=1.65nm and b=1.74 nm, 63340 atoms) networks as targets for a spherical (radius 5nm) rigid nanoparticle with initial kinetic energy K and mass of 10% of the studied graphene sheet (53463.6 amu, Figure 1c which collides with the center of the networks (Figure 1d). We have also carried out simulations for a graphene sheet (44553 atoms) for comparison purposes. The interaction between the incident particle and a carbon atom was modelled by a Lennard-Jones 12-6 potential.

The responses of the networks are shown in Figures 2-4 through various snapshots of the impact of a 5KeV nanoparticle. The collision causes a local deformation on the network generating a shock wave that propagates through it.
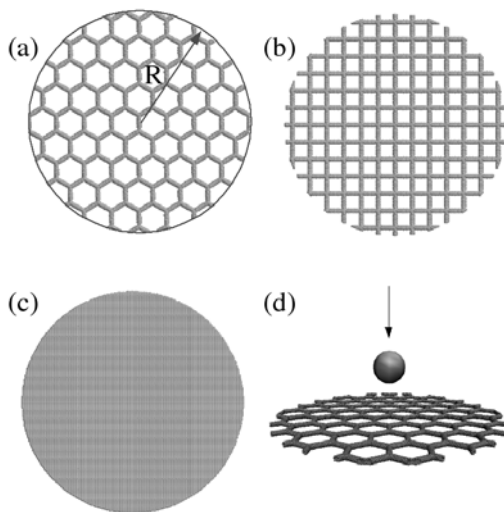
Figure 1. Networks models used in the impact molecular dynamics simulations. (a) a circular hexagonal network (Hex@(6,0), a=4.75nm; R=19nm), (b) a crossbar network (a=2.91nm and b=2.99nm), (c) a graphene sheet. (d) Representation of a spherical nanoparticle which will collide with the center of the network.

0 ps 2.5 ps 4.5 ps

5 ps 7.5 ps 9 ps

10 ps 12.5 ps 13.5ps
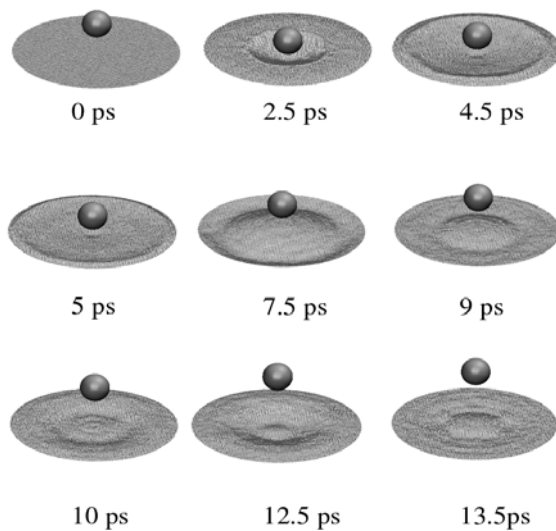
Figure 2. Snapshots of the impact of a 5KeV particle with the graphene sheet.
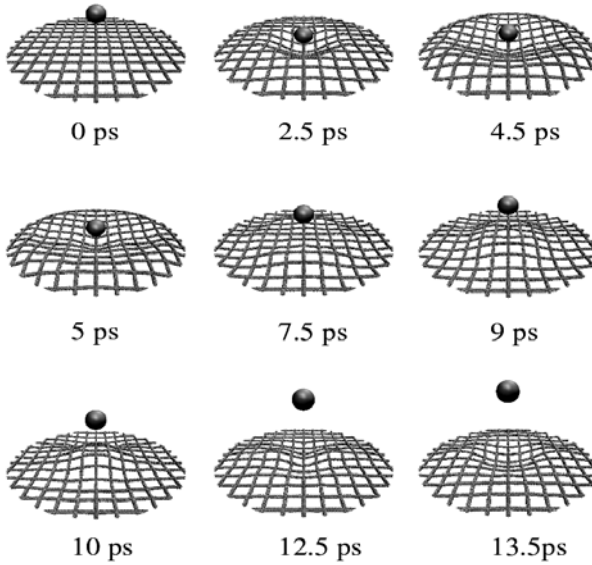
Figure 3. Snapshots of the impact of a 5KeV particle with a crossbar network.
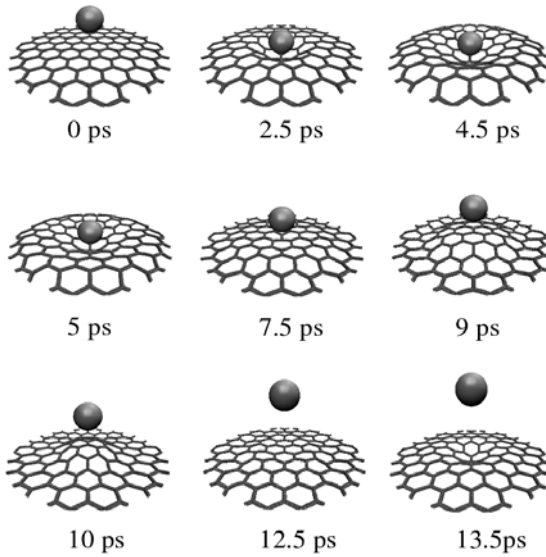
Figure 4. Snapshots of the impact of a 5KeV particle with the hexagonal network.

At about 2.5ps the particle is almost stopped and the deformation caused in the network propagates, reaches the borders and it is reflected. Approximately at about 5 ps the particle begins to be accelerated backward by the network when then, at about 9-10ps, it completely looses contact with the network.

4. Comparison between continuum and atomistic mechanics

The network responses to the colliding particle are analyzed by looking at the normal deformation Δz of the network calculated as the displacement of the particle from the point where it begins to interact with the network until the particle is completely stopped by it. Figure 5 presents the behavior of Δz^2 as a function of the initial kinetic energy of the incident particle, for the investigated three different nanotextures. Table 1 shows all the computed results, including two different types of crossbar and a disordered crossbar network.

The data can be fitted by the following expression $\Delta z^2 \propto K^s$, where s corresponds to the slope of the linear fits in the semi-log diagram of Figure 5. The values of s are reported in Table 1. For the graphene sheet, a single value of
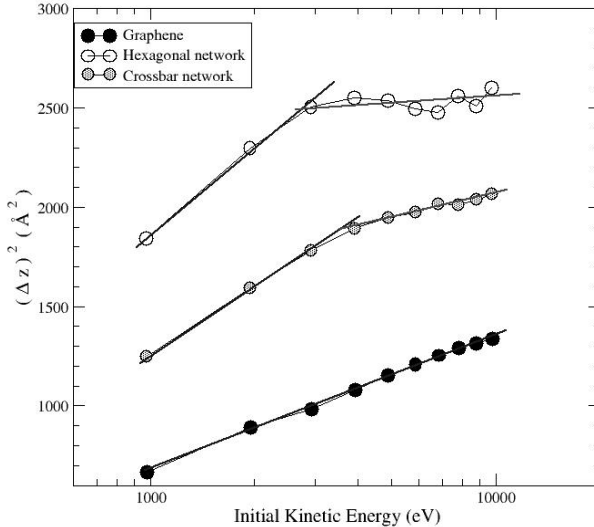
Figure 5. Behaviors of the squared normal deformation Δz^2 as a function of the initial kinetic energy of the incident particle. The targets are the ones shown in Figure 1. The straight lines are only guides to the eye.

Table 1. Behaviors of the squared normal deformation Δz^2 as a function of the initial kinetic energy of the incident particle. Transition(*) is not observed for graphene, thus it is expected for $K^* > 10KeV$, whereas in the other cases $K^* \approx$ 4-5KeV.

Graphene		Hexagonal		Crossbar $a=2.91nm$		Crossbar $a=1.65nm$		Disorder	
K [eV]	Δz^2 [Angs.²]	K [eV]	Δz^2 [Angs.²]	K [eV]	Δz^2 [Angs.²]	K [eV]	Δz^2 [Angs.²]	K [eV]	Δz^2 [Angs.²]
976.7	668.7	973.2	1841.3	974.4	1247.5	977.1	1179.1	975.7	1089.7
1953.4	891.6	1946.4	2299.2	1948.8	1593.6	1954.2	1495.3	1951.4	1393.5
2930.0	983.5	2919.6	2505.0	2923.3	1782.5	2931.3	1684.2	2927.2	1556.3
3906.7	1078.5	3892.8*	2550.3*	3897.7*	1894.0*	3908.4*	1801.9*	3902.9	1661.4
4883.3	1153.3	4865.9	2535.1	4872.1	1946.6	4886.2	1871.3	4879.3*	1728.1*
5860.0	1208.3	5839.2	2495.0	5846.6	1973.1	5862.8	1916.0	5854.4	1770.7
6836.7	1252.5	6812.4	2479.0	6820.9	2017.8	6839.9	1970.4	6830.1	1784.2
7813.3	1292.4	7785.6	2561.4	7795.4	2012.4	7816.9	1987.3	7805.9	1815.6
8790.0	1314.1	8758.8	2509.0	8769.8	2037.6	8794.1	2021.3	8781.6	1813.1
9768.3	1335.9	9735.5	2603.0	9745.8	2064.8	9772.7	2041.2	9758.9	1828.4
$s=0.30$ (bending) $s=---$ (stretching)		$s=0.28$ (bending) $s=0.01$ (stretching)		$s=0.31$ (bending) $s=0.08$ (stretching)		$s=0.33$ (bending) $s=0.14$ (stretching)		$s=0.31$ (bending) $s=0.08$ (stretching)	

$s \approx 0.3$ is sufficient to represent the data, at least in the range of the investigated initial kinetic energies. Note that, strictly speaking, this value is more close to that of stretching ($s = 1/2$) than to that of bending ($s =1$). Nevertheless, two different values $s \approx 0.3$ and $s \approx 0.1$ are necessary for the SWCNT networks. Larger values fit the behavior for lower initial energy regions while smaller ones to the behavior for higher energies.

These two different behaviors, associated with two different values of s, confirm the existence of the different response mechanisms, plausibly bending and stretching. In particular, as predicted by the model (Section 2), for small displacements we find $\Delta z^2 \propto K^s$, whereas for larger displacements $\Delta z^2 \propto K^{s/2}$. However, s is found to be close to 0.3 rather than to 1; this discrepancy remains an open question, if not simply imputable to the difference between continuum and atomistic mechanics. Moreover, note that the computed whole behavior includes both the stretching and bending as well as also the changes in the γ angles, the flattening of the nanotubes due to the perpendicular collision of the particle and so on. In spite of this the two theoretically predicted distinct mechanisms are clearly observed in the atomistic simulations.

In any case, the bending/stretching mechanisms are associated with changes of the angle γ formed by nanotubes and the junction (as a fishing net). The stretching regime is related to the axial stretching of the SWCNTs that form the network. For the low incident energy regime the main contribution to the deformation of the network would be caused by the "bending" mechanism. On the other hand, for the high energy regime, when the deformation angle is maximum (dictated by the network geometry), it is the stretching mechanism the responsible for the main behavior of the network. Since SWCNTs present a high Young's modulus in the axial direction, the energy associated with the stretching mechanism would be larger than that related to the bending one. Thus, it would be more difficult to change the position of the incident particle in the stretching regime, as observed in the simulations.

It is worth to notice that the global behavior would depend upon the network type, dimensions, and sheet shapes (circular in our case), as suggested by the analysis reported in Section 2, where l would describe a characteristic internal length of the nanotexture.

5. Conclusions

The existence of these well defined regimes suggests that the SWCNT nanotextures would present a high flexible behavior for small deformations perpendicularly applied to the network surface but would reach a "smart" less flexible state for larger deformations. Changing the nanotexture characteristics (architecture, nanotube type, unit cell dimensions, disorder) would tune the main mechanism type, as suggested by the analytical analysis, and, consequently, the mechanical properties presented by the nanotexture. Our findings could help in the design of nanotextures for futuristic flexible and tough.

Acknowledgements

References

1. Hoog, P. J., 2006, Science, 314, 1100.
2. Pugno, N. M., 2006, Acta Mat., 55, 1947.
3. Tan, V. B. C., Tay, T. E., Teo, W. K., 2005, Int. J. Solids and Structures, 42, 1561.
4. Pugno, N. M., 2006, Int. J of Fract., 140, 158.
5. Duan, H. L., Wang, J., Karihaloo, B. L., Huang, Z. P., 2006, Acta Mat., 54, 2983.

6. Diehl, M. R., Yaliraki, S. N., Beckman, R. A., Barahoma, M., Heath, J. R., 2002, Angew. Chem., 114, 363.

7. Derycke, V., Martel, R., Radosavljevic, M., Ross, F. M., Avouris, P., 2002, Nano Lett., 2, 1043.

8. Ago, H., Nakamura, K., Ikeda, K., Uehara, N., Ishigami, N., Tsuji, M., 2005, Chem. Phys. Lett., 408, 433.

9. Ismach, A., Joselevich, E., 2006, Nano Lett., 6, 1706.

10. Coluci, V. R., Dantas, S. O., Jorio, A., Galvão, D. S., 2007, Phys. Rev. B, 75, 075417.

11. Stuart, S. J., Tutein, A. B., Harrison, J. A., 2000, J. Chem. Phys.,112, 6472.

12. Brenner, D. W., 1990, Phys. Rev. B, 42, 9458.

13. Yakobson, B. I., Brabec, C. J., Bernholc, J., 1996, Phys. Rev. Lett. 76, 2511.

14. Zsoldos, I., Kakuk, G., Reti, T., Szasz, A., 2004, Mod. Sim. Mater. Sci. Eng. 12, 1251.

15. Srivastava, D., Saini, S., Menon, M., 1998, Ann. New York Acad. Sci., 852, 178.